Research Article

Spastin interacts with collapsin response mediator protein 3 to regulate neurite growth and branching

https://doi.org/10.4103/1673-5374.313052
Date of submission: August 31, 2020
Date of decision: October 26, 2020
Date of acceptance: February 6, 2021
Date of web publication: April 23, 2021

Zhi-Sheng Ji[1, #], Jian-Ping Li[2, #], Chao-Hua Fu[1, 3, #], Jian-Xian Luo[1], Hua Yang[1], Guo-Wei Zhang[1], Wutian Wu[2, 4, 5, *], Hong-Sheng Lin[1, *]

Graphical Abstract *Spastin and collapsin response mediator protein 3 (CRMP3) play roles in spinal cord injury and repair*

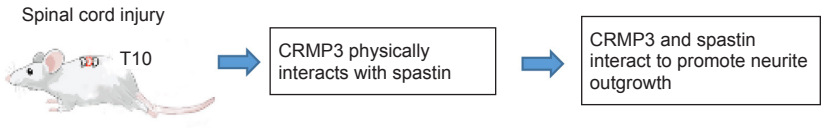

Abstract

Cytoskeletal microtubule rearrangement and movement are crucial in the repair of spinal cord injury. Spastin plays an important role in the regulation of microtubule severing. Both spastin and collapsin response mediator proteins can regulate neurite growth and branching; however, whether spastin interacts with collapsin response mediator protein 3 (CRMP3) during this process remains unclear, as is the mechanism by which CRMP3 participates in the repair of spinal cord injury. In this study, we used a proteomics approach to identify key proteins associated with spinal cord injury repair. We then employed liquid chromatography-mass spectrometry to identify proteins that were able to interact with glutathione S-transferase-spastin. Then, co-immunoprecipitation and staining approaches were used to evaluate potential interactions between spastin and CRMP3. Finally, we co-transfected primary hippocampal neurons with CRMP3 and spastin to evaluate their role in neurite outgrowth. Mass spectrometry identified the role of CRMP3 in the spinal cord injury repair process. Liquid chromatography-mass spectrometry pulldown assays identified three CRMP3 peptides that were able to interact with spastin. CRMP3 and spastin were co-expressed in the spinal cord and were able to interact with one another *in vitro* and *in vivo*. Lastly, CRMP3 overexpression was able to enhance the ability of spastin to promote neurite growth and branching. Therefore, our results confirm that spastin and CRMP3 play roles in spinal cord injury repair by regulating neurite growth and branching. These proteins may therefore be novel targets for spinal cord injury repair. The Institutional Animal Care and Use Committee of Jinan University, China approved this study (approval No. IACUS-20181008-03) on October 8, 2018.

Key Words: collapsin response mediator protein 3; liquid chromatography-mass spectrometry; microtubule; neurite growth; protein interactions; proteomics; spastin; spinal cord injury

Chinese Library Classification No. R453; R744; R363

Introduction

Acute traumatic spinal cord injury (SCI) can markedly and permanently degrade the quality of life of affected individuals (Tulsky et al., 2015). Initial SCI and associated trauma cause neuronal necrosis, which is followed by a secondary injury response that includes hemorrhage, excitotoxicity, elevated levels of intracellular calcium and free radicals, and fluid-electrolyte disturbances, ultimately resulting in additional neuronal death, glial scarring, and cavity formation (Gögel et al., 2010). The severing of axons within the spine or brain can result in permanent neurological deficits, as axonal regeneration does not readily occur in the adult central nervous system because of suppression mediated by microenvironmental and cell-autonomous factors (Dell'Anno and Strittmatter, 2017). This suggests that there may be shared mechanisms that inhibit axonal repair and govern axon repulsion in adults, although only limited overlap has been observed in molecular analyses (Sekine et al., 2019).

Collapsin response mediator proteins (CRMPs) are members of a family of heterotetrameric microtubule-associated proteins (CRMP1–5) (Lin et al., 2011; Khazaei et al., 2014; Niwa et al., 2017; He and Zhu, 2018), with CRMP2 being the most abundantly expressed member (Schmidt and Strittmatter, 2007; Zhang et al., 2019). CRMPs play important

[1]Department of Orthopedics, The First Affiliated Hospital of Jinan University, Guangzhou, Guangdong Province, China; [2]Guangdong-Hong Kong-Macau Institute of CNS Regeneration, Jinan University, Guangzhou, Guangdong Province, China; [3]Department of Orthopedics, Jiangmen Hospital of Sun Yat-sen University, Jiangmen, Guangdong Province, China; [4]Re-Stem Biotechnology Co., Ltd., Suzhou, Jiangsu Province, China; [5]Spine Surgery, The Third Affiliated Hospital of Sun Yat-sen University, Guangzhou, Guangdong Province, China
*Correspondence to: Wutian Wu, MD, PhD, wtwu@hkucc.hku.hk; Hong-Sheng Lin, MD, PhD, tlinhsh@jnu.edu.cn.
https://orcid.org/0000-0002-6945-8875 (Hong-Sheng Lin); https://orcid.org/0000-0001-2345-6789 (Wutian Wu)
#These authors contributed equally to this work.

Funding: *This work was supported by the National Natural Science Foundation of China, Nos. 31900691 (to GWZ), 81771331 (to HSL) and 81971165 (to WW); the National Basic Research Program of China (973 Program), No. 2014CB542205 (to WW); the Natural Science Foundation of Guangdong Province of China, No. 2017A030313595 (to HSL); the Science and Technology Program of Guangzhou, China, No. 201707010370 (to HSL); Project of Educational Commission of Guangdong Province of China, No. 2018KQNCX013 (to ZSJ); the Fundamental Research Funds for the Central Universities Project, China, No. 21618304 (to GWZ); Guangdong Provincial Key Research and Development Program "Precision Medicine and Stem Cell" Major Science and Technology Project, China, No. 3242001 (to WW); and China Postdoctoral Science Foundation, No. 2019M653292 (to ZSJ).*
How to cite this article: *Ji ZS, Li JP, Fu CH, Luo JX, Yang H, Zhang GW, Wu W, Lin HS (2021) Spastin interacts with collapsin response mediator protein 3 to regulate neurite growth and branching. Neural Regen Res 16(12):2549-2556.*

roles in neurotransmitter release, synaptic physiology (Chi et al., 2009), and regulating axonal growth in a range of contexts (Nagai et al., 2015; Takaya et al., 2017). CRMPs have also been suggested to be involved in myelin ligand signaling, and CRMP2 phosphorylation is essential for axonal degeneration in a murine model of experimental allergic encephalomyelitis (Petratos et al., 2012). CRMP also participates in the inhibition of myelin-associated glycoprotein-induced axon growth and Rho activation *in vitro* (Mimura et al., 2006). CRMP2 deletion can result in decreased cortical neuron spine density and a number of neuropsychiatric symptoms (Makihara et al., 2016; Nakamura et al., 2016). The deletion of CRMP2 specifically within the brain leads to memory and learning impairment (Zhang et al., 2016), consistent with the neuroprotective properties of this protein (Nagai et al., 2016). CRMPs are RhoA/Rho associated protein kinase 2 substrates downstream of NgR1 (Petratos et al., 2012), and certain CRMP isoforms are more likely to form hetero-oligomers than homotetramers (Deo et al., 2004).

Spastin is associated with the reconfiguration of microtubule branch points. When overexpressed, spastin enhances branch formation, while spastin depletion results in moderately decreased axon length as well as markedly decreased collateral branch formation (Yu et al., 2008; Lin et al., 2019). The ability of spastin to bind to microtubules is attributed to a 59-amino acid N-terminal microtubule-binding domain (Eckert et al., 2012). The ability of spastin to facilitate microtubule branching leads to more dynamic microtubules as a consequence of microtubule severing and increased availability of polymerizing terminals.

Cytoskeletal remodeling is a primary process in the regulation of neuronal morphology (Brody et al., 2015; Lei et al., 2016). Both spastin and CRMPs regulate axonal growth and branching and, while CRMP3 is closely associated with neuronal morphology (Gipson and Olive, 2017; Segal, 2017), the role of CRMP3 in the context of SCI remains to be established. It is also unknown whether CRMP3 and spastin interact with one another. As such, we herein assessed interactions between spastin and CRMP3 and their impact on neurite outgrowth in the context of SCI.

Materials and Methods

Animals

The Institutional Animal Care and Use Committee of Jinan University, China, approved this study (approval No. IACUS-20181008-03) on October 8, 2018. Sprague-Dawley rats (1-day-old; specific pathogen-free) and female Sprague-Dawley rats (180–220 g; 2.5-month-old; specific-pathogen-free) were purchased from the Experimental Animal Center of Sun Yat-sen University (license No. SYXK 2019-0209). All experiments were designed and reported according to the Animal Research: Reporting of *In Vivo* Experiments (ARRIVE) guidelines. The rats were randomized into sham (laminectomy only) and SCI (SCI induction at the T10 spinal segment) groups (n = 9/group). Rats were housed individually in a 25 ± 3°C facility with free food and water access.

SCI modeling

A rat model of SCI was established based on previously described methods (Wu et al., 2019). Briefly, rats were anesthetized by intraperitoneal injection of pentobarbital (32 mg/kg, Sinopharm Chemical Reagent Co., Ltd., Beijing, China), after which a 2.5 cm longitudinal dorsal incision was made exposing the T9–11 spinal processes and laminae. The entirety of the T10 lamina was then resected, and the exposed area of the spine was approximately 2.5 mm × 3 mm. Then, T10 facets were bilaterally fixed with a stabilizer. A U-shaped stabilizer (University of Louisville) with the rat was loaded onto the stage of a Louisville Injury System Apparatus (University of Louisville) and the dura/spinal cord height was adjusted directly under the impactor with guidance from the laser beam. Crash depth was adjusted to different damage levels, with crash depth set to 0.6, 1.0, or 1.8 mm for mild, moderate, and severe injuries, respectively, and with time set to 0.5 seconds (n = 9/group). The nitrogen tank controlling the impact tip was set at 18 psi or 124 kPa. After injury, the stabilizers were detached from the stage and rats were removed from the stabilizer. The injured area was assessed, and any bleeding was inhibited. Next, 3-0 silk sutures were used to suture muscles and skin. SCI model animals used in the final study met the following injury criteria: sluggish paralysis, a tail swaying reflex, flicking of the body and legs, spinal cord ischemia, and edema around the wound site (Jiang et al., 2014). Sham-operated animals underwent a T10 total laminectomy, but the spinal cord was not injured. All rats were treated with 2000 U/d gentamicin (Chongqing Xianfeng Animal Pharmaceutical Co. Ltd., Chongqing, China), and every 8 hours the bladder of each rat was squeezed manually to aid urination until spontaneous voiding was observed.

Liquid chromatography-mass spectrometry

Liquid chromatography-mass spectrometry (LC-MS) analyses of glutathione S-transferase (GST)-spastin pull-down assays were conducted by first resolving proteins from T10-centered spinal cord tissue samples on NuPAGE 4–12% gels (Life Technologies), followed by visualization with a Colloidal Blue Staining Kit (Life Technologies). Trypsin was used to digest excised protein bands and resulting peptides were analyzed by nanoflow reversed-phase liquid chromatography-tandem MS on a high-performance liquid chromatography Ultimate 5600 system (AB SCIEX, Framingham, CA, USA) connected to a linear ion trap (ThermoElectron, Waltham, MA, USA) in data-dependent acquisition mode.

Ingenuity pathway analysis and power law global error model analysis

Proteins identified by LC-MS as differentially expressed in injured spinal cord were subjected to ingenuity pathway analysis (IPA) (http://www.ingenuity.com) and power law global error model (PLGEM) analysis (Pavelka et al., 2004). These analyses utilized curated databases to identify overlapping functions and relationships among these proteins, assigning scores to specific biological functional networks. Scores > 2 typically indicate significant enrichment for a particular biological function among a given subset of proteins. These scores correspond to the log probability that a given network was detected solely due to random chance.

Heatmap generation and clustering

Proteins identified by LC-MS as differentially expressed in injured spinal cord and that were associated with enriched Gene Ontology (GO) terms were clustered and used to prepare heatmaps based on their log2 (transected/sham) fold-change values. The "Correlation (centered)" similarity metric in Cluster 3.0 was used to conduct hierarchical clustering, after which heatmaps were generated from output.cdt files with Java TreeView. The differentially expressed proteins were assessed by Kyoto Encyclopedia of Genes and Genomes (KEGG) and principal component analyses (Ma and Kosorok, 2009).

Pathological analysis

Rats were killed after intraperitoneal injection of pentobarbital (32 mg/kg), and then T10-centered spinal cord tissues were collected. Seventy-two hours post-injury, spinal cord tissues were collected for hematoxylin and eosin staining (Fan et al., 2020), immunofluorescence staining (Bai et al., 2021) and immunohistochemical staining as previously described (Wang et al., 2016). An area centered around T10 was observed. Briefly, a streptavidin-biotin complex kit (Jiehao, Shanghai, China) was used to stain sections. First, sections were incubated in 3% H_2O_2 at 37°C for 10 minutes to quench

endogenous peroxidase activity. Sections were then washed thrice with phosphate-buffered saline and blocked for 10 minutes with normal goat serum at 37°C prior to overnight incubation at 4°C with primary antibodies (rabbit polyclonal anti-CRMP3, 1:200, Cat# bs-11821R, Bioss, Beijing, China; mouse monoclonal anti-spastin, 1:1000, Cat# ab77144, Abcam, Cambridge, MA, USA; mouse monoclonal anti-glial fibrillary acidic protein, 1:1000, Cat# GB12096, Servicebio, Wuhan, China; rabbit polyclonal anti-myelin basic protein 1:1000, Cat# GB13226, Servicebio; goat polyclonal secondary antibody to Mouse IgG, Alexa Fluor 555, 1:1000, Cat# ab150118, Abcam; Goat polyclonal secondary antibody to rabbit, IgG, Alexa Fluor 488 1:1000, Cat# ab150077, Abcam). Next, samples were incubated with a horseradish peroxidase anti-rabbit IgG (1:200; Cat# KIT-5004; Fuzhou Maixin, Fuzhou, China) followed by incubation with horseradish peroxidase-conjugated-avidin at 37°C for 1 hour. Sections were then stained for 30 seconds using diaminobenzidine in phosphate-buffered saline, after which they were mounted onto glass slides, dehydrated with an ethanol gradient, treated with xylene, and coverslipped. Sections were then assessed via mild microscopy (Olympus, Tokyo, Japan), and Image Pro Plus 6.0 (Media Cybernetics, GA, USA) was used to quantify staining data.

Plasmid constructs and RNA interference

The CRMP3 sequence (NM_012933.1) was used to prepare a cDNA that was in turn cloned into pEGFP-C1 (Clontech, Palo Alto, CA, USA), pGEX-5x-3 (Amersham Pharmacia Biotech, Piscataway, NJ, USA) and pCMV-Tag2 (Stratagene, La Jolla, CA, USA). We additionally constructed GST-spastin. DNA sequencing was used to confirm all constructs. Validated spastin siRNA (siRNA Spastin) and scrambled sequence, negative control siRNA (siRNA NC) fragments were synthesized by Shanghai GenePharma (Shanghai, China).

GST pull-down assays

GST fusion protein pull-down assays were conducted as described previously (Ji et al., 2018). Briefly, whole spinal cord tissue was disrupted and lysed. GST-agarose beads (Invitrogen, Carlsbad, CA, USA) were rinsed, mixed with lysates, incubated for 1 hour at 4°C, and spun for 10 minutes at 1000 × *g* at 4°C. Supernatants were then collected and the above steps repeated once. Samples of approximately 400 μg were incubated with 200 μL protein-conjugated beads overnight at 4°C. Following a 5-minute spin at 1000 × *g* at 4°C, unbound proteins were removed by rinsing beads with 1 mL wash buffer, and then samples were spun for additional 1 minute at 1000 × *g* at 4°C. This wash step was repeated six times. Proteins that had been pulled down were analyzed by western blotting and MS.

Western blot assays and co-immunoprecipitation

Radioimmunoprecipitation assay buffer containing protease and phosphatase inhibitors (Roche, Basel, Switzerland) was used to lyse spinal cord or brain samples for western blot assays, while a non-denaturing lysis buffer [1% NP40, 5 mM ethylenediaminetetraacetic acid, 50 mM Tris-HCl (pH 8), 150 mM NaCl] containing the same inhibitors was used to lyse samples for co-immunoprecipitation. Samples were then separated via sodium dodecyl sulfate-polyacrylamide gel electrophoresis using 4–12% gels (Cat# V900859; Sigma-Aldrich, St. Louis, MO, USA). Protein bands were detected using enhanced chemiluminescence-Prime (Amersham, Buckinghamshire, UK) reagent. Densitometric analyses were conducted with Image Lab software (Bio-Rad, Hercules, CA, USA). Antibodies used for these analyses included anti-glyceraldehyde-3-phosphate dehydrogenase (mouse; 1:5000; Cat# GB12002; Servicebio), anti-CRMP3 (Cat# bs-11821R; 1:200; Bioss), anti-spastin (Cat# ab77144; 1:1000; Abcam), anti-horseradish peroxidase-conjugated goat anti-rabbit (1:5000; Cat# AS014; Abclonal Technology, Woburn, MA, USA), anti-horseradish peroxidase-conjugated goat anti-mouse (1:5000; Cat# AS003; Abclonal Technology), and anti-green fluorescent protein (GFP; 1:2000; Cat# ab290; Abcam). The primary antibody was incubated overnight at 4°C, and the secondary antibody was incubated at room temperature for one hour.

Cell culture and transfection

Hippocampal tissue was dissected from 1-day-old Sprague-Dawley rat pups. The rats were killed after intraperitoneal injection of pentobarbital (32 mg/kg), and then the brains were collected. Hippocampal neurons were dissociated with 0.125% trypsin (Cat# 25200-072; Gibco, Gaithersburg, MD, USA) and collected. These cells were then plated onto glass coverslips that had been coated with poly-D-lysine (Cat# P6407; Gibco) at 1×10^4 cells/cm^2, and were cultured in Neurobasal-A medium (Cat# 10888-022; Gibco) supplemented with 2% B27 (Cat# 17504044; Gibco) and 0.5 mM glutamine (Cat# 25030149; Gibco) at 37°C in a humidified 5% CO_2 incubator (Thermo, Waltham, MA, USA). Every three days, half of the cell culture medium was replaced. For appropriate experiments, hippocampal neurons were cultured *in vitro* for 48 hours and then transfected with recombinant plasmids via calcium phosphate transfection. To transfect neurons in 24-well tissue culture plates, 100 pmol of siRNA was combined with 37 μL of 2 M $CaCl_2$ solution in sterile, deionized water to a final volume of 300 μL and then mixed well with 300 μL 2× HEPES-buffered saline. To each well, 30 μL of this mixture was added drop-wise and incubated for another 25 minutes. After 24 hours, the neurons were fixed to observe cell morphology.

Cell morphology

Neurons were assessed using a Carl Zeiss LSM 700 confocal microscope (Zeiss, Jena, Germany) with a 63× oil objective at a 1024 × 1024 pixel resolution. Neuronal length and branching were calculated with the Image-Pro Plus program (Media Cybernetics, Silver Spring, MD, USA). Any neurites that had a length that was less than twice their diameter were excluded from the analyses.

Statistical analysis

SPSS v22.0 (IBM Corp., Armonk, NY, USA) was used for all statistical testing. Data are expressed as the mean ± standard deviation (SD), and were compared via Student's *t*-test. $P < 0.05$ was considered significant.

Results

Successful establishment of a rat SCI model

Rat models of SCI are the primary approach used to evaluate experimental treatments for this condition (Kjell and Olson, 2016). At 72 hours post-injury, hematoxylin and eosin-stained spinal cord sections from sham rats appeared smooth, whereas sections from SCI model rats exhibited evidence of edema, inflammatory cell infiltration, and consolidation of the spinal cord nucleus (**Figure 1A–D**). The spinal cord of sham animals was also smooth, whereas in SCI model rats it was uneven and hyperemic (**Figure 1B**). Immunofluorescence staining revealed glial fibrillary acidic protein (**Figure 1C**) and myelin basic protein (**Figure 1D**) immunopositivities in the normal central core at the site of surgery in the sham group, whereas the structure of this region in SCI model animals was highly disordered. In addition, Basso, Beattie & Bresnahan scores showed different degrees of behavioral ability consistent with the different levels of SCI inflicted (data not shown). Together, these findings indicate that we successfully established a rat model of SCI.

CRMP3 is involved in SCI

We next performed a proteomic analysis of spinal cord tissue samples from the model rats to identify key proteins associated with SCI (**Figure 2A**). This MS-based approach identified 3471 and 3213 proteins in the sham and SCI groups,

respectively, including 2783 (**Figure 2B**) and 2709 (**Figure 2C**) proteins that were identified in samples from the sham and SCI groups, respectively. IPA and PLGEM analyses identified 214 differentially expressed proteins associated with SCI, including 159 that were upregulated and 55 that were downregulated in injured spinal cord tissue. These differentially expressed proteins were then arranged in volcano plots and subjected to KEGG and principal component analyses (**Figure 3**). The sham and SCI groups could be clearly distinguished by principal component analysis, indicating that the SCI modeling was successful. PLGEM analysis revealed good repeatability among samples, while KEGG enrichment analysis indicated that the cytoskeleton signaling pathway was associated with SCI repair (**Figure 4A**). The microtubule-associated protein CRMP3 (DPYSL4) was among the top 10 downregulated proteins in this analysis (**Figure 4B**), and LC-MS analysis confirmed that CRMP3 protein expression was significantly lower in SCI model rats relative to sham controls (**Figure 4C**). Similar findings were also made via western blot assays (**Figure 4D** and **E**) and through immunofluorescence staining (**Figure 4F**), revealing that CRMP3 expression decreased as the degree of SCI increased. These findings thus provide strong evidence that CRMP3 is associated with SCI.

CRMP3 physically interacts with spastin

We next sought to identify which CRMP peptides were able to interact with spastin (**Figure 5**). Initially, GST-spastin was purified and used to pull-down interacting proteins within spinal cord lysates, after which these proteins were analyzed via LC-MS. Three CRMP peptides (SIPHITSDR, SAADIIALAR, and IAVGSDADVVIWDPDKMK) coming from the peptides identified by mass spectrometry were detected via LC-MS, confirming the ability of CRMPs to interact with GST-spastin.

To assess whether CRMP3 specifically interacts with spastin, we next purified CRMP3-GST and mixed it with spinal cord tissue lysates (**Figure 6A–E**). CRMP3-GST pull down assays revealed that while the GST control did not interact with spastin, the CRMP3-GST protein did (**Figure 6C**). This was confirmed via co-immunoprecipitation assays using rat spinal cord or brain lysis solution in which we were able to precipitate CRMP3 using a spastin-specific antibody, and to precipitate spastin using a CRMP3-specific antibody (**Figure 6A** and **B**). Immunofluorescence analysis also revealed co-localization of CRMP3 and spastin in the spinal cord, with the degree of this co-localization increasing to up to ~60% in the context of severe SCI (**Figure 6D** and **E**). These findings indicate that spastin and CRMP3 are co-expressed within the spinal cord and can interact with one another *in vitro* and *in vivo*.

CRMP3 and spastin synergistically promote neurite formation and outgrowth

Finally, we evaluated the ability of spastin and CRMP3 to interact in the context of neurite outgrowth. To that end, we co-transfected primary hippocampal neurons that had been grown *in vitro* for 2 days with GFP + mCherry (control), CRMP3-GFP (CRMP3) + Spastin-mCherry (spastin), CRMP3-GFP + siRNA Spastin, or CRMP3-GFP + siRNA NC (**Figure 7**). We have previously utilized siRNA constructs to assess the impact of spastin knockdown on neurite outgrowth and achieved ~92% spastin knockdown, which markedly inhibited such outgrowth (Ji et al., 2018). At 24 hours post-transfection, we harvested transfected neurites and quantified the length and total number of branching neurites. Significantly more branches were observed in CRMP3-GFP (CRMP3) + Spastin-mCherry (spastin) co-transfected neurons than in neurons of other groups ($P < 0.001$), and significantly more primary branches were observed among CRMP3 and spastin co-transfected neurons relative to CRMP3-GFP + siRNA Spastin co-transfected neurons. The number of second branches was also similar to the total number of branches. The total length of branches in CRMP3 and spastin co-transfected samples was significantly higher than that in the other three groups, while the CRMP3-GFP + siRNA NC group was also associated with increases in neuron length relative to controls (GFP + siRNA NC group), and the length of second branches in the CRMP3-GFP (CRMP3) + Spastin-mCherry (spastin) group was significantly increased compared with that in the other three groups ($P < 0.05$). Together, these findings clearly show that CRMP3 overexpression can enhance branch formation and neurite growth in the context of spastin expression, indicating synergistic interactions between these proteins.

Discussion

In this study, we found that CRMP3 was involved in SCI and interacts with spastin to drive neurite outgrowth. By identifying proteins that were differentially expressed in the context of SCI, we were able to determine that CRMP3 plays a role in this process, as evidenced by the fact that CRMP3 expression levels were inversely associated with the degree of SCI severity. We additionally found that spastin was able to physically interact with CRMP3 *in vivo* and *in vitro*, and that this interaction was conducive to neurite outgrowth. Together, these findings highlight a signal transduction pathway wherein CRMP3 and spastin work together to coordinate neurite branch formation and outgrowth.

Given that SCI is a leading cause of disability (LaPlaca et al., 2007), efforts to repair structural defects in the spinal cord arising due to injury or degeneration are central to the field of modern regenerative medicine (Friedli et al., 2015). Multiple pharmacological interventions have been designed to treat SCI and to aid in associated tissue repair based upon current understanding of the conditions necessary to promote nerve growth and to shape related inflammatory, immunological, and fibrotic responses. In combination with other cellular interventions, these treatments may render most SCIs curable in the near future (Silver et al., 2014; Watzlawick et al., 2016). However, it remains important that preclinical animal models of SCI be used in an effort to identify novel treatments for these debilitating injuries. At present, rat models of SCI are the primary means of experimentally evaluating SCI treatments *in vivo* (Reier et al., 2012; Gomes-Osman et al., 2016). As such, we established a rat model of SCI, generating rats with mild, moderate, and severely injured spinal cord tissue, as previously described (Cao et al., 2005).

Using an MS-based approach, we found the cytoskeletal signaling pathway to be closely associated with the process of SCI repair, as evidenced by KEGG enrichment analysis. This is consistent with prior studies demonstrating that the enhancement of microtubule stability can enhance SCI repair (Crunkhorn, 2015; Matamoros et al., 2019). As such, we sought to focus on SCI repair processes associated with the cytoskeleton. Our IPA analysis identified CRMP3 as a microtubule-associated protein that was among the 10 most down-regulated proteins in SCI model samples. We additionally confirmed that this protein was differentially regulated in the context of SCI via western blotting and immunofluorescence staining. CRMPs modulate microtubule dynamics so as to shape neuronal polarity (Fukata et al., 2002; Schmidt and Strittmatter, 2007). For example, CRMP2 is highly enriched in the growing axons of dissociated hippocampal cells (Inagaki et al., 2001), and CRMP2 post-translational modifications contribute to its ability to govern axonal regrowth after lesion (Gögel et al., 2010).

We provide clear evidence that spastin and CRMP3 are able to directly interact with one another. Spastin exists in two primary isoforms (spastin M1 and spastin M87), which are generated by two different translation initiation sites (Solowska et al., 2014). Spastin M87 is expressed at high levels in neural tissues (Goyal et al., 2014). We found exogenous spastin to be localized in clusters in the cytoplasm of neuronal cells, in

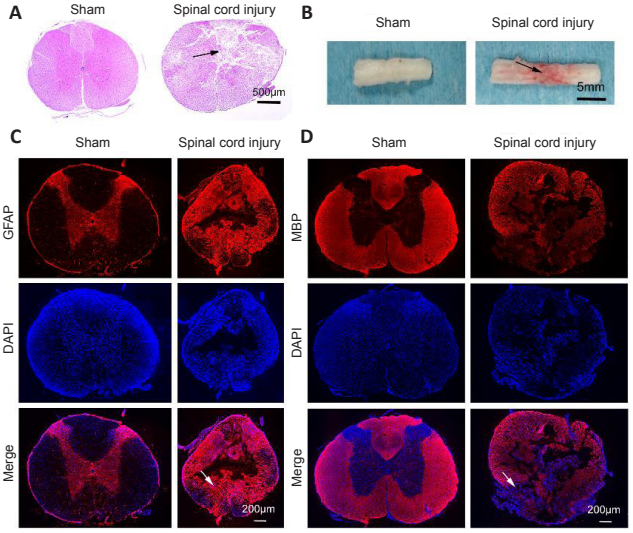

Figure 1 | **Rat spinal cord injury model establishment.**
(A) Spinal cord morphology in sham and spinal cord injury groups assessed by hematoxylin and eosin staining. Spinal cord sections of sham animals appeared smooth, whereas many cracks were apparent in those of spinal cord injury model animals (arrow). (B) The general morphology of the spinal cord. The spinal cord tissue of sham animals appeared smooth, whereas that of spinal cord injury model animals appeared uneven and hyperemic (arrow). (C, D) MBP (C) and GFAP (D) (red, Alexa Fluor 555) immunopositivities in spinal cord tissues. DAPI (blue) was used to stain nuclei. Sham rat sections appeared smooth, whereas sections from SCI model rats exhibited evidence of edema, inflammatory cell infiltration, and consolidation of the spinal cord nucleus. Scale bars: 500 μm in A, 5 mm in B, 200 μm in C and D. DAPI: 4′,6-Diamidino-2-phenylindole; GFAP: glial fibrillary acidic protein; MBP: myelin basic protein.

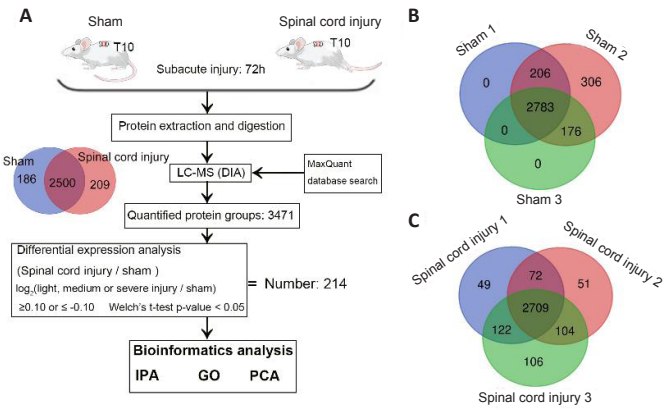

Figure 2 | **Proteomic identification of proteins associated with spinal cord injury.**
(A) An LC-MS approach was used to analyze spinal cord sections from sham and spinal cord injury model rats (n = 3/group) at 72 hours post-injury. In total, 3471 proteins were identified in these two groups, including 2500 that overlapped between both sample types. In total, we identified 214 differentially expressed proteins associated with spinal cord injury, after which IPA, GO, and PCA were used to functionally analyze these proteins. (B, C) Venn diagrams of the protein numbers in sham (B) and spinal cord injury (C) groups. In total, 3471 proteins were detected in sham samples, including 2783 that were detected in all three samples. In total, 3213 proteins were detected in spinal cord injury samples, including 2709 that were detected in all three samples. These analyses were repeated three times. DIA: Data independent acquisition; GO: gene ontology; IPA: ingenuity pathway analysis; LC-MS: liquid chromatography-mass spectrometry; PCA: principal component analysis.

line with previous findings (Finsterer et al., 2012). In addition, in injured spinal cord tissues, CRMP3 and spastin were co-localized with one another. These interactions indicate that both spastin and CRMP3 may play essential roles in regulating microtubule dynamics. The modular domain structure of spastin is similar to that of many other AAA (ATPases Associated with diverse cellular Activities) proteins (Lumb et al., 2012), and includes a C-terminal AAA ATPase domain, responsible for catalyzing the severing of microtubules, and an N-terminal microtubule-binding domain (Lumb et al., 2012). The N-terminal domain is responsible for interactions with certain adaptor proteins, which target spastin to specific sites of action within cells (Lumb et al., 2012). The spastin microtubule-binding domain is able to bind to microtubules in an ATP-independent fashion and is necessary for the severing of these microtubules (White et al., 2007). All CRMPs share a core 57–413 amino acid domain that is highly homologous to the amidohydrolase family member dihydropyrimidinase (DHP). This core domain contains the N-terminal domain, a DHPase domain, and a tubulin-binding domain (Zhang et al., 2007). CRMP3 is therefore likely to be able to directly interact with spastin, and as they both target microtubules, they may also interact with one another to govern microtubule dynamics.

In our final experiments, we provide evidence for synergistic interactions between CRMP3 and spastin in the regulation of neurite outgrowth. In prior analyses, we found that CRMP5 interacts with microtubules to control growth cone and neurite development (Ji et al., 2014), and there is evidence that CRMPs can control such neurite outgrowth by regulating microtubule polymerization and cargo transport. To date, however, no studies have assessed whether spastin and CRMP3 interact in this context to facilitate neurite outgrowth. As an AAA family protein, spastin is responsible for severing long microtubules into shorter subunits, thereby increasing the overall number and mobility of microtubules by increasing the distribution of their dynamic plus-ends. Spastin hexamerizes and docks onto these microtubules to sever them by interacting with the negatively charged C-terminal domain of tubulin in the central hexamer pore (Solowska and Baas, 2015). In line with past findings (Riano et al., 2009), we determined that spastin enhanced neurite branch formation and that spastin knockdown was sufficient to inhibit neurite outgrowth. We also found that CRMP3 was able to further enhance spastin-mediated induction of neurite branch formation and outgrowth when these two proteins were co-expressed in neurons. These findings thus indicate that spastin and CRMP3 interact with one another to control microtubule arrangement and neurite outgrowth.

In summary, our results indicate that CRMP3 and spastin are involved in SCI and that their interaction regulates neurite outgrowth, which may control SCI responses and related repair processes. However, how CRMP3 and spastin regulate protrusion growth in animals was not addressed in this study. As such, future studies of the importance of these interactions in the context of axon guidance mechanisms in the injured central nervous system may expedite efforts to achieve reliable and robust neural repair via appropriate therapeutic interventions.

Acknowledgments: *We thank University of Louisville for providing the U-shaped stabilizer and Louisville injury system apparatus.*
Author contributions: *Study conception and design: HSL, WW; experiment implementation: ZSJ, CHF, JPL; data acquisition: JPL, JXL, CHF; data analysis: ZSJ, HY, GWZ; manuscript writing: ZSJ. All authors reviewed and approved the final version of the manuscript.*
Conflicts of interest: *The authors declare that they have no known competing financial interests or personal relationships that could have appeared to influence the work reported in this paper. No conflicts of interest exist between Re-Stem Biotechnology Co., Ltd and publication of this paper.*
Financial support: *This work was supported by the National Natural Science Foundation of China, Nos. 31900691 (to GWZ), 81771331 (to HSL) and 81971165 (to WW); the National Basic Research Program of China (973 Program), No. 2014CB542205 (to WW); the Natural Science Foundation of Guangdong Province of China, No. 2017A030313595 (to HSL); the Science and Technology Program of Guangzhou, China, No. 201707010370 (to HSL); Project of Educational Commission of Guangdong Province of China, No. 2018KQNCX013 (to ZSJ); the Fundamental Research Funds for the Central Universities Project, China, No. 21618304 (to GWZ); Guangdong Provincial Key Research and Development Program "Precision Medicine and Stem Cell" Major Science and Technology Project, China, No. 3242001 (to WW); and China Postdoctoral Science Foundation, No. 2019M653292 (to ZSJ). The*

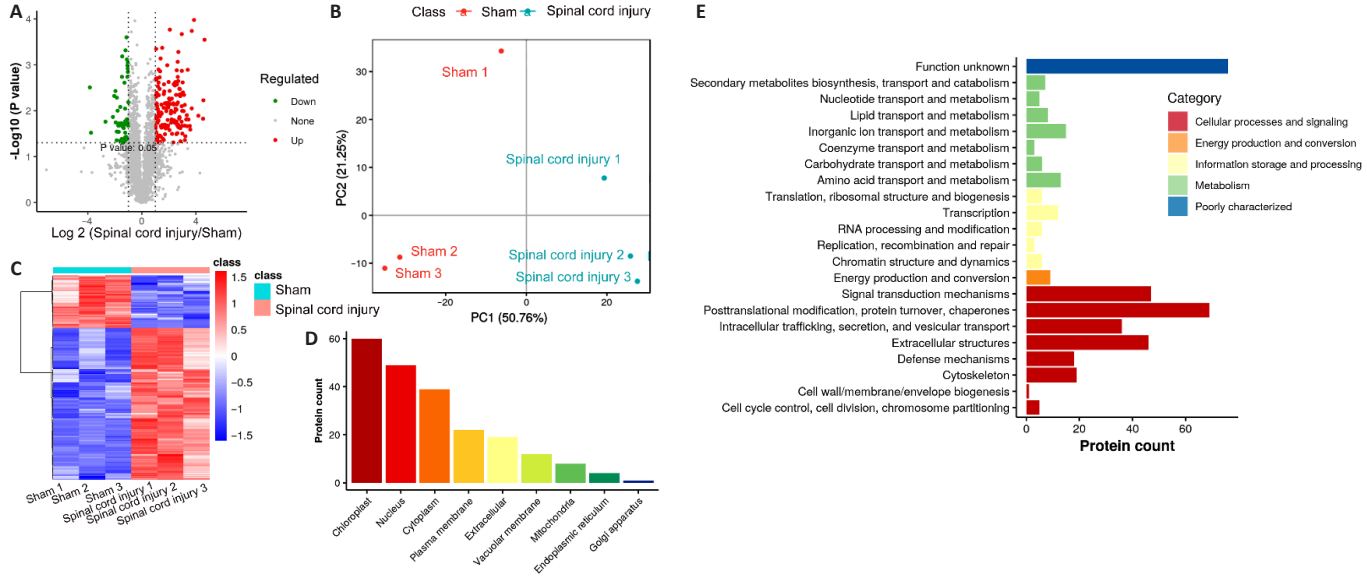

Figure 3 | **Analysis of differentially expressed proteins in injured rat spinal cord.**
(A) Volcano plots of detected proteins from liquid chromatography-mass spectrometry. Red and green dots correspond to upregulated and downregulated proteins, respectively. (B) Principal component analysis of six sham and spinal cord injury group samples, with components 1 and 2 represented on the two axes. This indicated that the spinal cord injury model was successful. (C) Presentation of differentially expressed proteins in a heatmap. Red represents high expression and blue represents low expression. (D) The subcellular localization of differentially expressed proteins. (E) Gene Ontology term enrichment for the differentially expressed proteins.

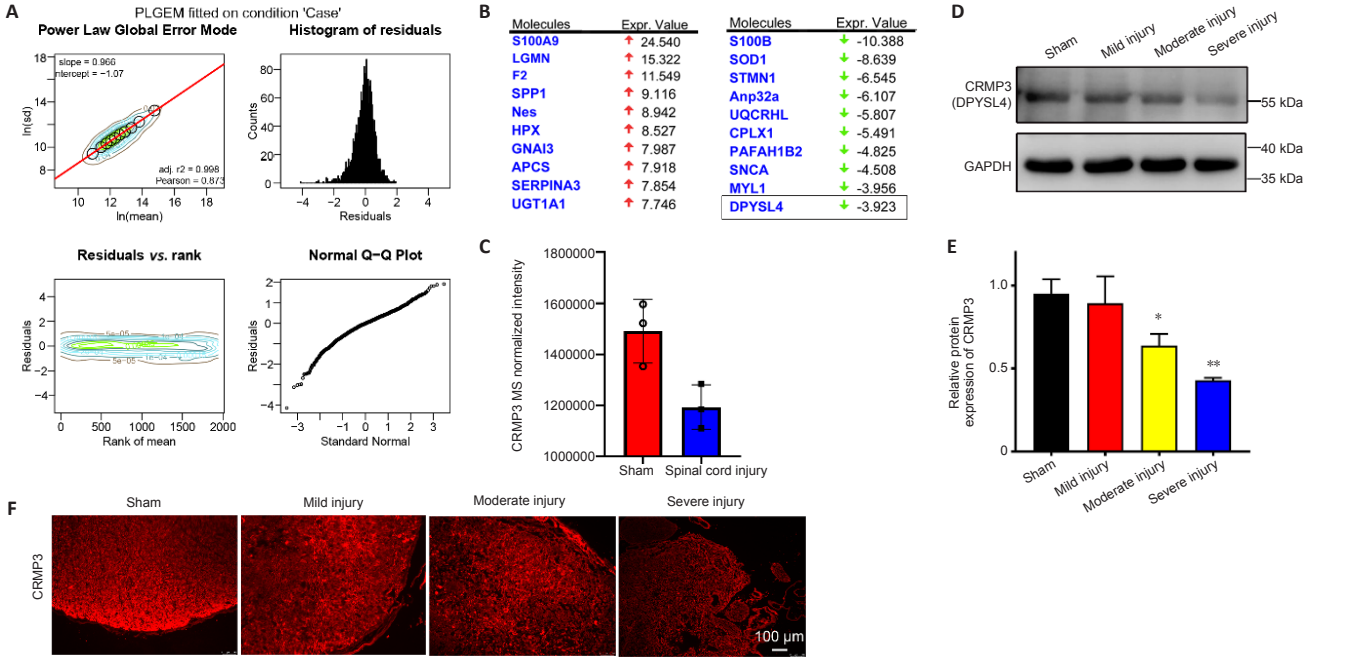

Figure 4 | **CRMP3 is involved in spinal cord injury.**
(A) PLGEM revealed equal goodness of fit for both sham and SCI datasets, with PLGEM modeling points shown in black on the corresponding contour plot. Red line corresponds to the PLGEM fitted to the indicated dataset. Residuals were calculated for each protein in a given dataset based upon the difference between the actual value and the PLGEM-predicted value and these residuals were plotted as a function of the rank of the row mean value and visualized using a contour plot. Distributions of residuals in the indicated contour plot are presented using a histogram to represent counts with equal-sized binning. Similarities between the distribution of residuals and the normal distribution are visualized with a quantile-quantile (Q-Q) plot. (B) The top 10 up- and down-regulated differentially expressed proteins from IPA analysis, identifying CRMP3 (DPYSL4) as a downregulated protein. (C) Relative expression of CRMP3 in LC-MS analysis of sham and SCI group samples. (D) CRMP3 (DPYSL4) was detected by western blotting of spinal cord from rats with SCI of different severities, with GAPDH used as a loading control (n = 3/group). (E) Quantification of CRMP3 protein expression levels by western blot analysis. Data are expressed as the mean ± SD (n = 3 rats in each group). *P < 0.05, **P < 0.01, *vs.* sham group (Student's t-test). (F) CRMP3 immunopositivity (red, Alexa Fluor 555) was detected via immunofluorescence staining, revealing that CRMP3 expression decreased as the degree of SCI increased. Scale bar: 100 μm. CRMP3: Collapsin response mediator protein; GAPDH: glyceraldehyde-3-phosphate dehydrogenase; IPA: ingenuity pathway analysis; LC-MS: liquid chromatography-mass spectrometry; PLGEM: power law global error model.

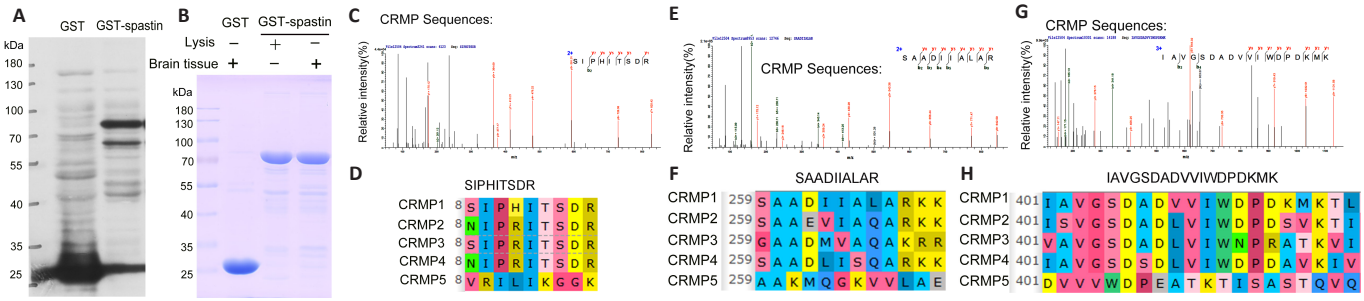

Figure 5 | **CRMP peptides interact with spastin.**
(A) GST-spastin was purified and detected via western blotting. (B) GST and GST-spastin pull-down assays were conducted with spinal cord lysates. (C, E, G) LC-MS was used to detect products that could interact with GST-spastin. Three CRMP peptides (SIPHITSDR, SAADIIALAR, and IAVGSDADVVIWDPDKMK) were identified. (D, F, H) Significant homology is evident among CRMP1–5 for the three detected peptides, indicating that CRMPs interact with spastin. CRMP: Collapsin response mediator protein; GST: glutathione S-transferase; LC-MS: liquid chromatography-mass spectrometry.

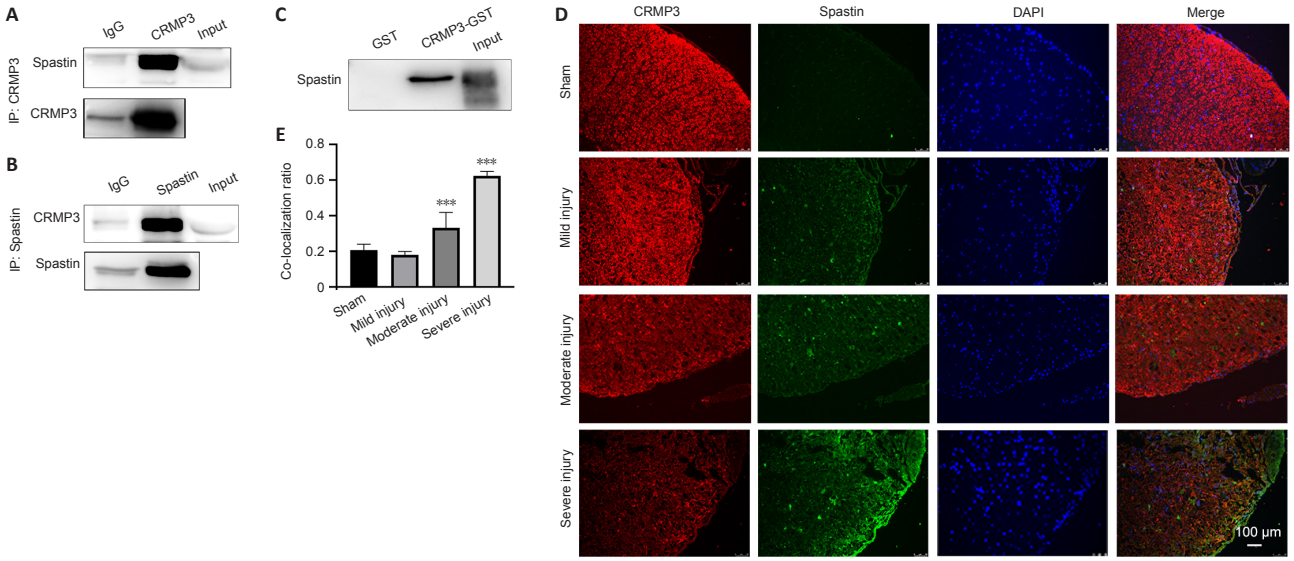

Figure 6 | **CRMP3 physically interacts with spastin in brain and spinal cord tissue of a rat spinal cord injury model.**
(A, B) Proteins precipitated using anti-CRMP3 (A) and anti-spastin (B) antibodies were detected with anti-spastin and anti-CRMP3 antibodies, respectively. (C) GST and GST-CRMP3 pull-downs were conducted using enriched brain lysates. (D) Spastin and CRMP3 co-localized in spinal cord tissues to varying degrees depending on injury severity. Increased spinal cord injury correlated with decreased CRMP3 and increased spastin expression (n = 3/group). Spastin, CRMP3, and DAPI are shown in red (Alexa Fluor 555), green (Alexa Fluor 488), and blue, respectively, with merged sections shown in yellow. Images are representative of at least three experiments. Scale bar: 100 μm. (E) Co-localization ratio of CRMP3 and spastin, which reflects the severity of spinal cord injury. Data are expressed as the mean ± SD (n = 3 rats in each group). ***P < 0.001, *vs.* sham group (Student's t-test). CRMP3: Collapsin response mediator protein 3; DAPI: 4′,6-diamidino-2-phenylindole; IP: immunoprecipitation.

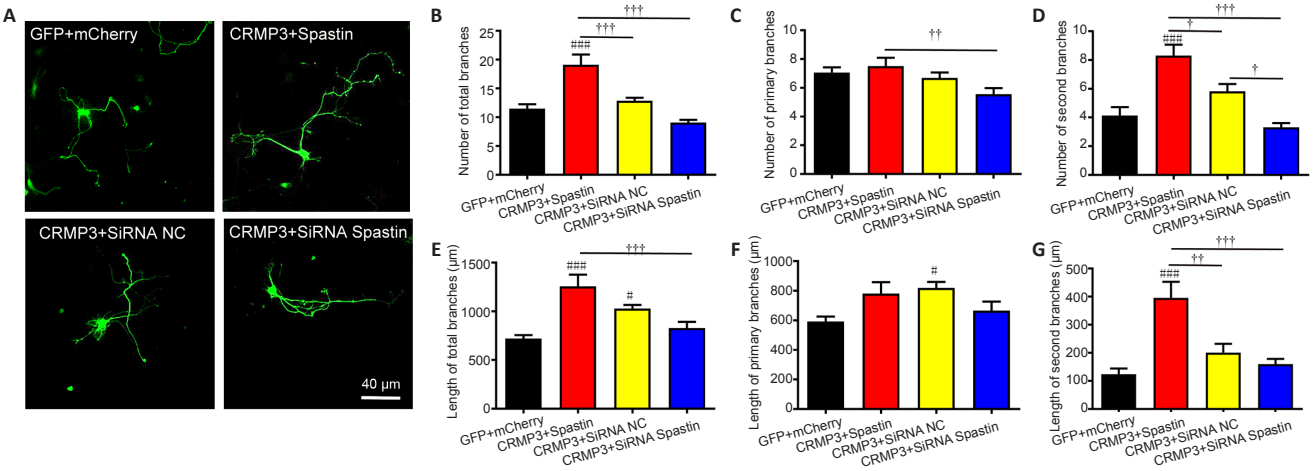

Figure 7 | **CRMP3 and spastin interact to promote neurite outgrowth.**
(A) After *in vitro* culture for 2 days, hippocampal neurons were co-transfected with GFP/mCherry, CRMP3/spastin, CRMP3/siRNA Spastin, or CRMP3/siRNA NC for 24 hours. Scale bar: 40 μm. (B–D) Numbers of total (B), primary (C), and secondary (D) branches were quantified, revealing that CRMP3 and spastin interacted to promote branch formation (n = 15/group). (E–G) The length of total (E), primary (F), and secondary (G) branches, revealing that spastin and CRMP3 interacted to promote neurite outgrowth (n = 15/group). Data are expressed as the mean ± SD from triplicate experiments. #P < 0.05, ###P < 0.001, *vs.* GFP + mCherry group; †P < 0.05, ††P < 0.01, †††P < 0.001 (Student's t-test). CRMP3: Collapsin response mediator protein 3; GFP: green fluorescent protein; NC: negative control; siRNA: small interfering RNA.

funding sources had no role in study conception and design, data analysis or interpretation, paper writing or deciding to submit this paper for publication.
Institutional review board statement: *This study was approved by Institutional Animal Care and Use Committee of Jinan University, China (approval No. IACUS-20181008-03) on October 8, 2018.*
Copyright license agreement: *The Copyright License Agreement has been signed by all authors before publication.*
Data sharing statement: *Datasets analyzed during the current study are available from the corresponding author on reasonable request.*
Plagiarism check: *Checked twice by iThenticate.*
Peer review: *Externally peer reviewed.*
Open access statement: *This is an open access journal, and articles are distributed under the terms of the Creative Commons Attribution-NonCommercial-ShareAlike 4.0 License, which allows others to remix, tweak, and build upon the work non-commercially, as long as appropriate credit is given and the new creations are licensed under the identical terms.*
Open peer reviewers: *Olga Kopach, University College London, UK; Hirokazu Ohtaki, Showa University, Japan; Xiaoming Jin, Indiana University, USA.*
Additional file: *Open peer review reports 1–3.*

References

Bai W, Li M, Xu W, Zhang M (2021) Comparison of effects of high- and low-frequency electromagnetic fields on proliferation and differentiation of neural stem cells. Neurosci Lett 741:135463.
Brody DL, Benetatos J, Bennett RE, Klemenhagen KC, Mac Donald CL (2015) The pathophysiology of repetitive concussive traumatic brain injury in experimental models; new developments and open questions. Mol Cell Neurosci 66:91-98.
Cao Q, Zhang YP, Iannotti C, DeVries WH, Xu XM, Shields CB, Whittemore SR (2005) Functional and electrophysiological changes after graded traumatic spinal cord injury in adult rat. Exp Neurol 191 Suppl 1:S3-16.
Chi XX, Schmutzler BS, Brittain JM, Wang Y, Hingtgen CM, Nicol GD, Khanna R (2009) Regulation of N-type voltage-gated calcium channels (Cav2.2) and transmitter release by collapsin response mediator protein-2 (CRMP-2) in sensory neurons. J Cell Sci 122:4351-4362.
Crunkhorn S (2015) CNS injury: Microtubule stabilizer repairs spinal cord injury. Nat Rev Drug Discov 14:310.
Dell'Anno MT, Strittmatter SM (2017) Rewiring the spinal cord: direct and indirect strategies. Neurosci Lett 652:25-34.
Deo RC, Schmidt EF, Elhabazi A, Togashi H, Burley SK, Strittmatter SM (2004) Structural bases for CRMP function in plexin-dependent semaphorin3A signaling. EMBO J 23:9-22.
Eckert T, Le DT, Link S, Friedmann L, Woehlke G (2012) Spastin's microtubule-binding properties and comparison to katanin. PLoS One 7:e50161.
Fan L, Li X, Liu T (2020) Asiaticoside inhibits neuronal apoptosis and promotes functional recovery after spinal cord injury in rats. J Mol Neurosci 70:1988-1996.
Finsterer J, Löscher W, Quasthoff S, Wanschitz J, Auer-Grumbach M, Stevanin G (2012) Hereditary spastic paraplegias with autosomal dominant, recessive, X-linked, or maternal trait of inheritance. J Neurol Sci 318:1-18.
Friedli L, Rosenzweig ES, Barraud Q, Schubert M, Dominici N, Awai L, Nielson JL, Musienko P, Nout-Lomas Y, Zhong H, Zdunowski S, Roy RR, Strand SC, van den Brand R, Havton LA, Beattie MS, Bresnahan JC, Bezard E, Bloch J, Edgerton VR, et al. (2015) Pronounced species divergence in corticospinal tract reorganization and functional recovery after lateralized spinal cord injury favors primates. Sci Transl Med 7:302ra134.
Fukata Y, Itoh TJ, Kimura T, Ménager C, Nishimura T, Shiromizu T, Watanabe H, Inagaki N, Iwamatsu A, Hotani H, Kaibuchi K (2002) CRMP-2 binds to tubulin heterodimers to promote microtubule assembly. Nat Cell Biol 4:583-591.
Gipson CD, Olive MF (2017) Structural and functional plasticity of dendritic spines- root or result of behavior? Genes Brain Behav 16:101-117.
Gögel S, Lange S, Leung KY, Greene ND, Ferretti P (2010) Post-translational regulation of Crmp in developing and regenerating chick spinal cord. Dev Neurobiol 70:456-471.
Gomes-Osman J, Cortes M, Guest J, Pascual-Leone A (2016) A systematic review of experimental strategies aimed at improving motor function after acute and chronic spinal cord injury. J Neurotrauma 33:425-438.
Goyal U, Renvoisé B, Chang J, Blackstone C (2014) Spastin-interacting protein NA14/SSNA1 functions in cytokinesis and axon development. PLoS One 9:e112428.
He J, Zhu J (2018) Collapsin response mediator protein-2 ameliorates sevoflurane-mediated neurocyte injury by targeting PI3K-mTOR-S6K pathway. Med Sci Monit 24:4982-4991.
Inagaki N, Chihara K, Arimura N, Ménager C, Kawano Y, Matsuo N, Nishimura T, Amano M, Kaibuchi K (2001) CRMP-2 induces axons in cultured hippocampal neurons. Nat Neurosci 4:781-782.
Ji Z, Tan M, Gao Y, Zhang J, Gong X, Guo G, Lin H (2014) CRMP-5 interacts with tubulin to promote growth cone development in neurons. Int J Clin Exp Med 7:67-75.
Ji Z, Zhang G, Chen L, Li J, Yang Y, Cha C, Zhang J, Lin H, Guo G (2018) Spastin interacts with CRMP5 to promote neurite outgrowth by controlling the microtubule dynamics. Dev Neurobiol 78:1191-1205.
Jiang SH, Tu WZ, Zou EM, Hu J, Wang S, Li JR, Wang WS, He R, Cheng RD, Liao WJ (2014) Neuroprotective effects of different modalities of acupuncture on traumatic spinal cord injury in rats. Evid Based Complement Alternat Med 2014:431580.
Khazaei MR, Girouard MP, Alchini R, Ong Tone S, Shimada T, Bechstedt S, Cowan M, Guillet D, Wiseman PW, Brouhard G, Cloutier JF, Fournier AE (2014) Collapsin response mediator protein 4 regulates growth cone dynamics through the actin and microtubule cytoskeleton. J Biol Chem 289:30133-30143.
Kjell J, Olson L (2016) Rat models of spinal cord injury: from pathology to potential therapies. Dis Model Mech 9:1125-1137.
LaPlaca MC, Simon CM, Prado GR, Cullen DK (2007) CNS injury biomechanics and experimental models. Prog Brain Res 161:13-26.
Lei W, Omotade OF, Myers KR, Zheng JQ (2016) Actin cytoskeleton in dendritic spine development and plasticity. Curr Opin Neurobiol 39:86-92.
Lin PC, Chan PM, Hall C, Manser E (2011) Collapsin response mediator proteins (CRMPs) are a new class of microtubule-associated protein (MAP) that selectively interacts with assembled microtubules via a taxol-sensitive binding interaction. J Biol Chem 286:41466-41478.
Lin YF, Xie Z, Zhou J, Chen HH, Shao WW, Lin HD (2019) Effect of exogenous spastin combined with polyethylene glycol on sciatic nerve injury. Neural Regen Res 14:1271-1279.
Lumb JH, Connell JW, Allison R, Reid E (2012) The AAA ATPase spastin links microtubule severing to membrane modelling. Biochim Biophys Acta 1823:192-197.
Ma S, Kosorok MR (2009) Identification of differential gene pathways with principal component analysis. Bioinformatics 25:882-889.
Makihara H, Nakai S, Ohkubo W, Yamashita N, Nakamura F, Kiyonari H, Shioi G, Jitsuki-Takahashi A, Nakamura H, Tanaka F, Akase T, Kolattukudy P, Goshima Y (2016) CRMP1 and CRMP2 have synergistic but distinct roles in dendritic development. Genes Cells 21:994-1005.
Matamoros AJ, Tom VJ, Wu D, Rao Y, Sharp DJ, Baas PW (2019) Knockdown of fidgetin improves regeneration of injured axons by a microtubule-based mechanism. J Neurosci 39:2011-2024.
Mimura F, Yamagishi S, Arimura N, Fujitani M, Kubo T, Kaibuchi K, Yamashita T (2006) Myelin-associated glycoprotein inhibits microtubule assembly by a Rho-kinase-dependent mechanism. J Biol Chem 281:15970-15979.
Molina AE, Cristante AF, de Barros TE, Sr., Molina MS, Molina TP (2015) A computerized system for the application of Basso, Beattie and Bresnahan scale in Wistar rats. Acta Ortop Bras 23:179-183.
Nagai J, Owada K, Kitamura Y, Goshima Y, Ohshima T (2016) Inhibition of CRMP2 phosphorylation repairs CNS by regulating neurotrophic and inhibitory responses. Exp Neurol 277:283-295.
Nagai J, Kitamura Y, Owada K, Yamashita N, Takei K, Goshima Y, Ohshima T (2015) Crmp4 deletion promotes recovery from spinal cord injury by neuroprotection and limited scar formation. Sci Rep 5:8269.
Nakamura H, Yamashita N, Kimura A, Kimura Y, Hirano H, Makihara H, Kawamoto Y, Jitsuki-Takahashi A, Yonezaki K, Takase K, Miyazaki T, Nakamura F, Tanaka F, Goshima Y (2016) Comprehensive behavioral study and proteomic analyses of CRMP2-deficient mice. Genes Cells 21:1059-1079.
Niwa S, Nakamura F, Tomabechi Y, Aoki M, Shigematsu H, Matsumoto T, Yamagata A, Fukai S, Hirokawa N, Goshima Y, Shirouzu M, Nitta R (2017) Structural basis for CRMP2-induced axonal microtubule formation. Sci Rep 7:10681.
Pavelka N, Pelizzola M, Vizzardelli C, Capozzoli M, Splendiani A, Granucci F, Ricciardi-Castagnoli P (2004) A power law global error model for the identification of differentially expressed genes in microarray data. BMC Bioinformatics 5:203.
Petratos S, Ozturk E, Azari MF, Kenny R, Lee JY, Magee KA, Harvey AR, McDonald C, Taghian K, Moussa L, Mun Aui P, Siatskas C, Litwak S, Fehlings MG, Strittmatter SM, Bernard CC (2012) Limiting multiple sclerosis related axonopathy by blocking Nogo receptor and CRMP-2 phosphorylation. Brain 135:1794-1818.
Reier PJ, Lane MA, Hall ED, Teng YD, Howland DR (2012) Translational spinal cord injury research: preclinical guidelines and challenges. Handb Clin Neurol 109:411-433.
Riano E, Martignoni M, Mancuso G, Cartelli D, Crippa F, Toldo I, Siciliano G, Di Bella D, Taroni F, Bassi MT, Cappelletti G, Rugarli EI (2009) Pleiotropic effects of spastin on neurite growth depending on expression levels. J Neurochem 108:1277-1288.
Schmidt EF, Strittmatter SM (2007) The CRMP family of proteins and their role in Sema3A signaling. Adv Exp Med Biol 600:1-11.
Segal M (2017) Dendritic spines: Morphological building blocks of memory. Neurobiol Learn Mem 138:3-9.
Sekine Y, Algarate PT, Cafferty WBJ, Strittmatter SM (2019) Plexina2 and CRMP2 signaling complex is activated by Nogo-A-liganded Ngr1 to restrict corticospinal axon sprouting after trauma. J Neurosci 39:3204-3216.
Silver J, Schwab ME, Popovich PG (2014) Central nervous system regenerative failure: role of oligodendrocytes, astrocytes, and microglia. Cold Spring Harb Perspect Biol 7:a020602.
Solowska JM, Baas PW (2015) Hereditary spastic paraplegia SPG4: what is known and not known about the disease. Brain 138:2471-2484.
Solowska JM, D'Rozario M, Jean DC, Davidson MW, Marenda DR, Baas PW (2014) Pathogenic mutation of spastin has gain-of-function effects on microtubule dynamics. J Neurosci 34:1856-1867.
Takaya R, Nagai J, Piao W, Niisato E, Nakabayashi T, Yamazaki Y, Nakamura F, Yamashita N, Kolattukudy P, Goshima Y, Ohshima T (2017) CRMP1 and CRMP4 are required for proper orientation of dendrites of cerebral pyramidal neurons in the developing mouse brain. Brain Res 1655:161-167.
Tulsky DS, Kisala PA, Victorson D, Tate DG, Heinemann AW, Charlifue S, Kirshblum SC, Fyffe D, Gershon R, Spungen AM, Bombardier CH, Dyson-Hudson TA, Amtmann D, Kalpakjian CZ, Choi SW, Jette AM, Forchheimer M, Cella D (2015) Overview of the spinal cord injury--quality of life (SCI-QOL) measurement system. J Spinal Cord Med 38:257-269.
Wang X, Shi SH, Yao HJ, Jing QK, Mo YP, Lv W, Song LY, Yuan XC, Li ZG, Qin LN (2016) Electroacupuncture at Dazhui (GV14) and Mingmen (GV4) protects against spinal cord injury: the role of the Wnt/β-catenin signaling pathway. Neural Regen Res 11:2004-2011.
Watzlawick R, Rind J, Sena ES, Brommer B, Zhang T, Kopp MA, Dirnagl U, Macleod MR, Howells DW, Schwab JM (2016) Olfactory ensheathing cell transplantation in experimental spinal cord injury: effect size and reporting bias of 62 experimental treatments: a systematic review and meta-analysis. PLoS Biol 14:e1002468.
White SR, Evans KJ, Lary J, Cole JL, Lauring B (2007) Recognition of C-terminal amino acids in tubulin by pore loops in Spastin is important for microtubule severing. J Cell Biol 176:995-1005.
Wu X, Qu W, Bakare AA, Zhang YP, Fry CME, Shields LBE, Shields CB, Xu XM (2019) A laser-guided spinal cord displacement injury in adult mice. J Neurotrauma 36:460-468.
Yu W, Qiang L, Solowska JM, Karabay A, Korulu S, Baas PW (2008) The microtubule-severing proteins spastin and katanin participate differently in the formation of axonal branches. Mol Biol Cell 19:1485-1498.
Zhang H, Kang E, Wang Y, Yang C, Yu H, Wang Q, Chen Z, Zhang C, Christian KM, Song H, Ming GL, Xu Z (2016) Brain-specific Crmp2 deletion leads to neuronal development deficits and behavioural impairments in mice. Nat Commun 7:11773.
Zhang Z, Ottens AK, Sadasivan S, Kobeissy FH, Fang T, Hayes RL, Wang KK (2007) Calpain-mediated collapsin response mediator protein-1, -2, and -4 proteolysis after neurotoxic and traumatic brain injury. J Neurotrauma 24:460-472.
Zhang ZY, Yang J, Fan ZH, Wang DL, Wang YY, Zhang T, Yu LM, Yu CY (2019) Fresh human amniotic membrane effectively promotes the repair of injured common peroneal nerve. Neural Regen Res 14:2199-2208.

P-Reviewers: Kopach O, Ohtaki H, Jin X; C-Editor: Zhao M; S-Editors: Yu J, Li CH; L-Editors: Yu J, Song LP; T-Editor: Jia Y